Applied Ocean Research 56 (2016) 67–78

Contents lists available at ScienceDirect

Applied Ocean Research

journal homepage: www.elsevier.com/locate/apor

Bragg reflection of water waves by multiple submerged semi-circular breakwaters

Yong Liu [a,*], Hua-jun Li [a], Lei Zhu [b]

[a] Shandong Provincial Key Laboratory of Ocean Engineering, Ocean University of China, Qingdao 266100, China
[b] Qinhuangdao Mineral Resource and Hydrogeological Brigade, Hebei Geological Prospecting Bureau, Qinhuangdao 066001, China

ARTICLE INFO

Article history:
Received 18 August 2015
Received in revised form 5 December 2015
Accepted 21 January 2016
Available online 10 February 2016

Keywords:
Semi-circular breakwaters
Bragg reflection
Multipole expansions
Experimental tests

ABSTRACT

This study examines the Bragg reflection of water waves by multiple submerged semi-circular breakwaters. The multipole expansions combined with the shift of polar coordinates are used to develop full linear potential solutions of the problem. In the full solutions, the obliquely and normally incident waves are independently considered. Experimental tests are carried out to measure the reflection and transmission coefficients of the breakwaters at different wave periods and body spacings. The analytical results are in reasonable agreement with the experimental data. The peak reflection coefficient of multiple submerged semi-circular breakwaters and the bandwidth of Bragg reflection are carefully examined by numerical examples. Some significant results for practical application are discussed.

1. Introduction

Breakwaters submerged in the sea have the merits of not affecting coastal aesthetics and allowing water circulation and fish passage. Thus, the submerged breakwaters have been often used for providing partial sheltering to coastlines and coastal structures. To enhance the sheltering function, multiple parallel breakwaters may be built. When the wave number component k_x in the normal direction of the parallel breakwaters and the breakwater spacing D satisfy the relation of $k_xD = n\pi$ ($n = 1, 2, \ldots$), the wave reflection can be amplified significantly, which is the so-called Bragg reflection. This study will examine the Bragg reflection of water waves by multiple submerged semi-circular breakwaters.

Bragg reflections of water waves over natural periodic sea beds or sandbars have been well studied by many researchers. Davies and Heathershaw [1] and Mei [2] examined the Bragg reflection of normally incident surface waves by periodic sandbars based on theoretical analysis and experimental tests. Kirby [3] developed a general wave equation for wave motions over rippled beds by extending Berkhoff's mild-slope equation. Mei et al. [4] studied the Bragg reflection of obliquely incident waves by sinusoidal sandbars, and found the zero reflection of bars at a critical incident angle of $\pi/4$. Guazzelli et al. [5] developed a theoretical model for the higher-order Bragg reflection of normally incident waves by periodic beds using integral matching methods, in which the slope bottom was discretized into successive steps and the eigenfunction solutions of velocity potentials in all step regions were obtained [6,7]. The integral matching methods were also used by Rey [8] and Cho and Lee [9] for analysing oblique wave reflection by either sinusoidal beds or structures. Athanassoulis and Belibassakis [10] derived a coupled-mode theory for water wave propagation over variable bathymetry regions, which could completely describe the influence of the bottom slope. Porter and Porter [11] used integral equation techniques to examine the behaviour of water waves over periodic beds.

As for artificial ocean structures, Mei et al. [4] proposed the concept of building a series of submerged bars to protect the drilling platforms in the Ekofisk of the North Sea from storm wave attack. Hence, more studies on the Bragg reflections of submerged breakwaters have been carried out. Belzons et al. [12] presented experimental evidence of the localization phenomenon for water waves over a large number of rectangular bars, which were randomly placed on the water bottom. Mattioli [13] confirmed the appearance of Bragg reflection by a series of submerged rectangular bars using matched eigenfunction expansion solution. Mattioli [13] also showed that compared to plane waves, the evanescent modes near the rectangular bars reduced the resonant frequency. Bailard et al. [14] demonstrated that a series of submerged artificial humps with suitable spacings and heights could provide storm erosion protection along U.S. Gulf Coast and Atlantic Coast beaches. Mase et al. [15] numerically and experimentally studied water wave motion over a series of trapezoidal porous bars. Their results showed that

* Corresponding author at: College of Engineering, Ocean University of China, No. 238 Song-ling Road, Qingdao 266100, China. Tel.: +86 532 66781129; fax: +86 532 66781550.
E-mail address: liuyong_77@hotmail.com (Y. Liu).

http://dx.doi.org/10.1016/j.apor.2016.01.008
0141-1187/

the Bragg reflection also occurred for multiple porous structures. Hsu et al. [16] enhanced the reflecting performance of multiple submerged rectangular bars by setting non-identical bar spacings. Cho et al. [17] compared the reflection coefficients of multiple submerged rectangular and trapezoidal bars based on calculated and experimental results, and indicated that the trapezoidal bars are better for reflecting waves. Twu and Liu [18] and Lan et al. [19] developed eigenfunction expansion solutions for Bragg reflections of water waves by rigid and elastic rectangular porous bars, respectively. Zhang et al. [20] numerically examined the porous seabed response near two and three submerged trapezoidal bars due to the Bragg reflection. Recently, Karmakar and Guedes Soares [21] developed an analytical solution for the Bragg reflection of water waves by multiple submerged porous thin barriers. Liu et al. [22] developed linear analytical solutions for long wave resonant reflections by multiple submerged bars with different shapes, including triangular, rectified cosinoidal and trapezoidal shapes. They also presented curves to determine the optimal collocations of these Bragg reflection breakwaters.

In preceding studies, the Bragg reflection breakwaters with different shapes have been carefully examined. But, the Bragg reflection of multiple semi-circular caissons has not been studied to the authors' knowledge. The first semi-circular caisson breakwater was built at Miyazaki Port, Japan in early 1990s [23]. The major merits of semi-circular caissons were summarized by Xie [24] as follows: zero overturning moment acting on the caisson as the wave pressure acting on the semi-circular arc passes through the circle centre; higher stability against sliding compared to vertical structures; and easy for building and removal. Due to these merits, the semi-circular caissons have been widely used for building breakwaters and jetties in China since 1997. In practice, the semi-circular caissons may be impermeable or permeable, and the semi-circular caisson breakwaters can be submerged or surface-piercing according to different requirements. Mallayachari and Sundar [25] developed a boundary element method solution for normally incident linear water wave motion over a single submerged semi-circular bar. Yuan and Tao [26] and Zhang et al. [27] examined the hydrodynamic performance of a single semi-circular breakwater based on numerical simulations and experimental tests, respectively. Dhinakaran et al. [28] reviewed relevant studies on semi-circular breakwaters. Liu and Li [29,30] analysed normally and obliquely incident wave actions on a single submerged permeable semi-circular breakwater using multipole expansions [31–35].

Since the semi-circular caissons have intrinsic merits as mentioned above, it may be a good idea to build multiple semi-circular bars to serve as the Bragg reflection breakwater. The present study will use analytical and experimental methods to examine the Bragg reflection of water waves by multiple submerged semi-circular breakwaters, and give some significant results for engineering applications. In the following section, the boundary-value problem of water wave scattering by multiple submerged semi-circular breakwaters is formulated. In Section 3, accurate full solutions for the present problem are developed using the multipole expansions combined with the shift of polar coordinates, where the obliquely and normally incident waves are independently considered. The experimental tests are introduced in Section 4. In Section 5, the full solutions, the wide-spacing approximations and the experimental data are compared. Numerical examples are also presented to examine the effects of major parameters on the Bragg reflection. Finally, the main conclusions of this study are drawn.

2. Mathematical formulation

As shown in Fig. 1, we consider water wave scattering by a series of semi-circular breakwaters (bars) submerged in the ocean with a constant depth h. We define a Cartesian coordinate system with the x-axis along the still water level and the z-axis pointing vertically upwards. There are total N semi-circular bars, and the radius of bar p is a_p ($p = 1, 2, \ldots, N$). The centre of bar p is located at $(x_p, -h)$ and $x_1 = 0$. The local polar coordinate system about the centre of bar p is defined with $r_p \sin\theta_p = x - x_p$ and $r_p \cos\theta_p = -(z+h)$. In the p-th polar coordinate system, the centre of bar q ($q \neq p$) is located at (R_{pq}, α_{pq}), where $R_{pq} = |x_q - x_p| > (a_q + a_p)$, $\alpha_{pq} = \pi/2$ for $q > p$, and $\alpha_{pq} = 3\pi/2$ for $q < p$. The spacing between adjacent bar centres is $D_p = x_{p+1} - x_p$ ($p = 1, 2, \ldots, N-1$). The incident waves from $x = -\infty$ propagate at an angle β to the x-axis. The length of each semi-circular bar in the y-direction is very long compared to the wavelength and thus is assumed to be infinite.

We examine the present water wave scattering problem in the context of linear potential theory. The fluid is assumed to be inviscid and incompressible, and that its motion is irrotational. Then, we can use a velocity potential $\Phi(x, y, z, t)$ to describe the fluid motion. For time-harmonic waves with angular frequency ω, the velocity potential can be further written as:

$$\Phi(x, y, z, t) = Re\left\{-\frac{igH}{2\omega}\frac{1}{\cosh(kh)}\phi(x, z)e^{-ik_y y}e^{-i\omega t}\right\}, \tag{1}$$

where Re denotes the real part of argument; $i = \sqrt{-1}$; g is the acceleration due to gravity; H is the incident wave height; $\phi(x, z)$ is a reduced spatial velocity potential; $k_y = k\sin\beta$; and k is the incident wave number, which satisfies

$$K = \frac{\omega^2}{g} = k\tanh(kh). \tag{2}$$

The velocity potential $\phi(x, z)$ satisfies the modified Helmholtz equation:

$$\frac{\partial^2\phi}{\partial x^2} + \frac{\partial^2\phi}{\partial z^2} - k_y^2\phi = 0. \tag{3}$$

The velocity potential also satisfies the free surface condition, the far field radiation conditions, and the impermeable conditions on the seabed and bar surfaces:

$$\frac{\partial\phi}{\partial z} = K\phi, \quad z = 0, \tag{4}$$

$$\lim_{x\to\pm\infty}\left(\frac{\partial}{\partial x} \mp ik_x\right)(\phi - \phi_I) = 0, \tag{5}$$

$$\frac{\partial\phi}{\partial z} = 0, \quad z = -h, \tag{6}$$

$$\frac{\partial\phi}{\partial r_p} = 0, \quad r_p = a_p, \quad p = 1, 2, \ldots, N, \tag{7}$$

where $k_x = k\cos\beta$; and ϕ_I is the velocity potential of incident waves given by

$$\phi_I = \cosh(k(z+h))e^{ik_x x}. \tag{8}$$

The above incident wave potential satisfies Eqs. (3)–(6).

Now, a complete boundary-value problem for wave scattering by multiple submerged semi-circular breakwaters is formulated in terms of Eqs. (3)–(8). In the following section, we will find the full solutions of velocity potentials using multipole expansions combined with the shift of polar coordinates. The obliquely and normally incident waves will be independently solved.

3. Multipole expansion solutions

3.1. Obliquely incident wave solution

Multipoles are singular solutions of governing Eq. (3) with boundary conditions in Eqs. (4)–(6). The Multipoles singular at $(x,$

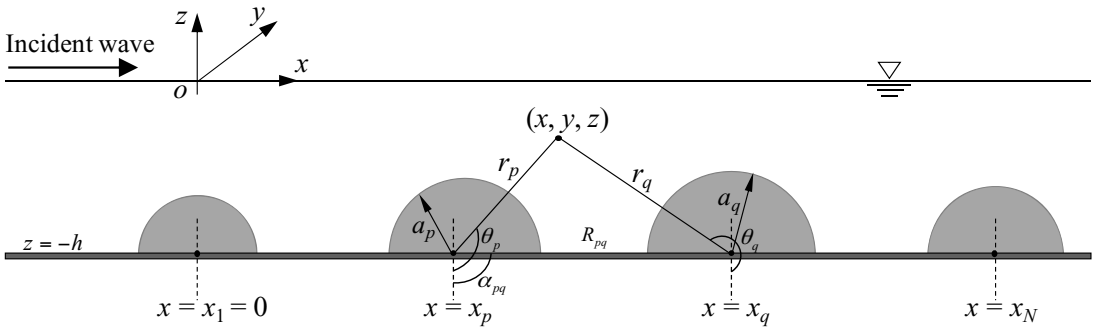

Fig. 1. Sketch for wave scattering by multiple submerged semi-circular breakwaters.

$z) = (x_p, -h)$ and symmetric and antisymmetric in θ_p are respectively given by [30,36]:

$$\begin{aligned}\varphi^+_{p,n} &= K_{2n}(k_y r_p)\cos(2n\theta_p) \\ &+ \int_0^\infty \hbar(\nu)\cosh(2n\mu)\,\cos(k_y(x-x_p)\,\sinh\,\mu)\,\cosh(\nu(z+h)) \\ &\mathrm{d}\mu, \quad n \geq 0, \\ &= K_{2n}(k_y r_p)\cos(2n\theta_p) + \sum_{m=0}^{\infty} A^+_{pp,mn} I_{2m}(k_y r_p)\,\cos(2m\theta_p),\end{aligned} \tag{9}$$

$$\begin{aligned}\varphi^-_{p,n} &= K_{2n-1}(k_y r_p)\,\sin((2n-1)\theta_p) \\ &+ \int_0^\infty \hbar(\nu)\,\sinh((2n-1)\mu)\,\sin(k_y(x-x_p)\,\sinh\,\mu) \\ &\cosh(\nu(z+h))\,\mathrm{d}\mu, \quad n \geq 1, \\ &= K_{2n-1}(k_y r_p)\,\sin((2n-1)\theta_p) \\ &+ \sum_{m=1}^{\infty} B^-_{pp,mn} I_{2m-1}(k_y r_p)\,\sin((2m-1)\theta_p),\end{aligned} \tag{10}$$

with

$$\hbar(\nu) = \frac{(K+\nu)\mathrm{e}^{-\nu h}}{\nu\,\sinh(\nu h) - K\,\cosh(\nu h)}, \tag{11}$$

$$A^+_{pp,mn} = \varepsilon_m \int_0^\infty \hbar(\nu)\,\cosh(2n\mu)\,\cosh(2m\mu)\,\mathrm{d}\mu, \tag{12}$$

$$B^-_{pp,mn} = 2\int_0^\infty \hbar(\nu)\,\sinh((2n-1)\mu)\,\sinh((2m-1)\mu)\,\mathrm{d}\mu, \tag{13}$$

where $\nu = k_y \cosh\mu$; K_n and I_n are modified Bessel functions of the first and second kinds of order n, respectively; $\varepsilon_0 = 1$ and $\varepsilon_m = 2$ $(m \geq 1)$; and the path of each integration passes beneath the pole at $\mu = \kappa = \ln(1/\sin\beta + \sqrt{1/\sin^2\beta - 1})$ to satisfy the far field radiation conditions [37,38]. The computational methods of such types of integrals in Eqs. (12) and (13) can be found in Linton [39, Eq. (4.11)].

The velocity potential, which satisfies Eqs. (3)–(6), can be written as the sum of the incident wave potential and all the multipoles:

$$\phi = \phi_I + \sum_{p=1}^{N}\left(\sum_{n=0}^{\infty}\xi^+_{p,n}\varphi^+_{p,n} + \sum_{n=1}^{\infty}\xi^-_{p,n}\varphi^-_{p,n}\right), \tag{14}$$

where $\xi^+_{p,n}$ and $\xi^-_{p,n}$ are unknown complex coefficients. Now, we can use impermeable bar surface condition in Eq. (7) to determine the unknown coefficients. To impose this condition, we must write the incident wave potential and all the multipoles in terms of each local polar coordinate.

By using the generating function of modified Bessel function [40, Eqs. (8.511-4) and (8.406-3)], the velocity potential of incident waves can be rewritten as

$$\phi_I = \mathrm{e}^{\mathrm{i}k_x x_q}\left[\begin{array}{l}\displaystyle\sum_{n=0}^{\infty}\varepsilon_n\,\cosh(2n\kappa)I_{2n}(k_y r_q)\,\cos(2n\theta_q) \\ \displaystyle +2\mathrm{i}\sum_{n=1}^{\infty}\sinh((2n-1)\kappa)I_{2n-1}(k_y r_q)\,\sin((2n-1)\theta_q)\end{array}\right]. \tag{15}$$

To shift the polar coordinate from bar p to bar q, we need use the Graf's addition theorem [40, Eq. (8.530)]:

$$K_n(k_y r_p)\mathrm{e}^{\mathrm{i}n\theta_p} = \sum_{m=-\infty}^{\infty}(-1)^m K_{n+m}(k_y R_{pq})I_m(k_y r_q)\mathrm{e}^{-\mathrm{i}m\theta_q}\mathrm{e}^{\mathrm{i}(n+m)\alpha_{pq}}, \quad r_q < R_{pq}, \quad p \neq q. \tag{16}$$

Then, the multipoles in Eqs. (9) and (10) are rewritten as

$$\begin{aligned}\varphi^+_{p,n} &= \sum_{m=0}^{\infty} A^+_{pq,mn} I_{2m}(k_y r_q)\cos(2m\theta_q) \\ &+ \sum_{m=1}^{\infty} B^+_{pq,mn} I_{2m-1}(k_y r_q)\quad \sin((2m-1)\theta_q), \quad p \neq q,\end{aligned} \tag{17}$$

$$\begin{aligned}\varphi^-_{p,n} &= \sum_{m=0}^{\infty} A^-_{pq,mn} I_{2m}(k_y r_q)\cos(2m\theta_q) \\ &+ \sum_{m=1}^{\infty} B^-_{pq,mn} I_{2m-1}(k_y r_q)\sin((2m-1)\theta_q), \quad p \neq q,\end{aligned} \tag{18}$$

with

$$A^+_{pq,mn} = P^+_{pq,mn} + R^+_{pq,mn}, B^+_{pq,mn} = Q^+_{pq,mn} - S^+_{pq,mn}, \quad p \neq q, \tag{19}$$

$$A^-_{pq,mn} = P^-_{pq,mn} + R^-_{pq,mn}, B^-_{pq,mn} = Q^-_{pq,mn} + S^-_{pq,mn}, \quad p \neq q, \tag{20}$$

where

$$P^+_{pq,mn} = (-1)^{n+m}\frac{\varepsilon_m}{2}[K_{2n+2m}(k_y R_{pq}) + K_{2n-2m}(k_y R_{pq})], \tag{21}$$

$$\begin{aligned}P^-_{pq,mn} &= (-1)^{n+m+1}\frac{\varepsilon_m}{2}\,\mathrm{sgn}(q-p)[K_{2n+2m-1}(k_y R_{pq}) \\ &+ K_{2n-2m-1}(k_y R_{pq})],\end{aligned} \tag{22}$$

$$Q^+_{pq,mn} = (-1)^{n+m}\,\mathrm{sgn}(q-p)[K_{2n+2m-1}(k_y R_{pq}) + K_{2n-2m+1}(k_y R_{pq})], \tag{23}$$

$$Q^{-}_{pq,mn} = (-1)^{n+m+1}[K_{2n+2m-2}(k_yR_{pq}) + K_{2n-2m}(k_yR_{pq})], \tag{24}$$

$$R^{+}_{pq,mn} = \varepsilon_m \int_0^{\infty} \hbar(\nu)\cosh(2n\mu) \cosh(2m\mu)\cos(k_yR_{pq}\ \sinh u)\,\mathrm{d}\mu, \tag{25}$$

$$R^{-}_{pq,mn} = \varepsilon_m \,\mathrm{sgn}(q-p) \int_0^{\infty} \hbar(\nu)\sinh((2n-1)\mu) \cosh(2m\mu)\sin(k_yR_{pq}\ \sinh u)\,\mathrm{d}\mu, \tag{26}$$

$$S^{+}_{pq,mn} = 2\mathrm{sgn}(q-p) \int_0^{\infty} \hbar(\nu)\cosh(2n\mu)\ \ \sinh((2m-1)\mu) \sin(k_yR_{pq}\ \sinh u)\,\mathrm{d}\mu, \tag{27}$$

$$S^{-}_{pq,mn} = 2 \int_0^{\infty} \hbar(\nu)\sinh((2n-1)\mu)\sinh((2m-1)\mu) \cos(k_yR_{pq}\ \sinh u)\,\mathrm{d}\mu, \tag{28}$$

For the simplicity of expressions below, we further define

$$A^{-}_{pp,mn} = B^{+}_{pp,mn} = 0. \tag{29}$$

Inserting the velocity potential in Eq. (14) into Eq. (7), and using Eqs. (9), (10), (15), (17) and (18), we get N sets of new equations. Multiplying both sides of each new equation by $\cos(2m\theta_q)$ or $\sin((2m-1)\theta_q)$, and then integrating with respect to θ_q from $\pi/2$ to $3\pi/2$, we have for $q = 1, 2, \ldots, N$:

$$\xi^{+}_{q,m}Z_{2m} + \sum_{p=1}^{N}\left(\sum_{n=0}^{\infty}\xi^{+}_{p,n}A^{+}_{pq,mn} + \sum_{n=1}^{\infty}\xi^{-}_{p,n}A^{-}_{pq,mn}\right) = -\varepsilon_m\ \cosh(2m\kappa)\mathrm{e}^{\mathrm{i}k_xx_q}, \quad m \geq 0, \tag{30}$$

$$\xi^{-}_{q,m}Z_{2m-1} + \sum_{p=1}^{N}\left(\sum_{n=0}^{\infty}\xi^{+}_{p,n}B^{+}_{pq,mn} + \sum_{n=1}^{\infty}\xi^{-}_{p,n}B^{-}_{pq,mn}\right) = -2\mathrm{i}\ \sinh((2m-1)\kappa)\mathrm{e}^{\mathrm{i}k_xx_q}, \quad m \geq 1, \tag{31}$$

where $Z_m = K'_m(k_ya_q)/I'_m(k_ya_q)$ and the prime denotes the derivative with respect to k_yr_q. Finally, a $(2M+1)N \times (2M+1)N$ system is obtained and solved by truncating m and n to M according to desired accuracy.

When $x \to \pm\infty$, the multipoles become [30, Eqs. (37) and (38)]:

$$\varphi^{+}_{p,n} \sim \frac{\mathrm{i}\pi\ \cosh(2n\kappa)}{2k_xN_0h}\mathrm{e}^{\mp\mathrm{i}k_xx_p}\ \cosh(k(z+h))\mathrm{e}^{\pm\mathrm{i}k_xx}, \tag{32}$$

$$\varphi^{-}_{p,n} \sim \pm\frac{\pi\ \sinh((2n-1)\kappa)}{2k_xN_0h}\mathrm{e}^{\mp\mathrm{i}k_xx_p}\ \cosh(k(z+h))\mathrm{e}^{\pm\mathrm{i}k_xx}, \tag{33}$$

where

$$N_0 = \frac{1}{2} + \frac{\sinh(2kh)}{4kh}. \tag{34}$$

Thus, the magnitudes of complex reflection and transmission coefficients for multiple semi-circular bars, C_R and C_T, are calculated by

$$C_R = |\tilde{R}| = \left|\sum_{p=1}^{N}\mathrm{e}^{\mathrm{i}k_xx_p}\left[\sum_{n=0}^{\infty}\xi^{+}_{p,n}\frac{\mathrm{i}\pi\ \cosh(2n\kappa)}{2k_xN_0h} - \sum_{n=1}^{\infty}\xi^{-}_{p,n}\frac{\pi\ \sinh((2n-1)\kappa)}{2k_xN_0h}\right]\right|, \tag{35}$$

$$C_T = |\tilde{T}| = \left|1 + \sum_{p=1}^{N}\mathrm{e}^{-\mathrm{i}k_xx_p}\left[\sum_{n=0}^{\infty}\xi^{+}_{p,n}\frac{\mathrm{i}\pi\ \cosh(2n\kappa)}{2k_xN_0h} + \sum_{n=1}^{\infty}\xi^{-}_{p,n}\frac{\pi\ \sinh((2n-1)\kappa)}{2k_xN_0h}\right]\right|. \tag{36}$$

The conservation of wave energy gives

$$C_R^2 + C_T^2 = 1. \tag{37}$$

3.2. Normally incident wave solution

For normally incident waves ($\beta = 0$, $k_y = 0$ and $k_x = k$), the modified Helmholtz equation becomes 2D Laplace equation. We can still use Eq. (14) to represent the velocity potential by removing the term of $n = 0$. But, the multipoles for normally incident waves are given by [29,36]:

$$\begin{aligned}\varphi^{+}_{p,n} &= \frac{\cos(2n\theta_p)}{r_p^{2n}} + \frac{1}{(2n-1)!}\int_0^{\infty}\hbar(\mu)\mu^{2n-1}\ \cosh(\mu(z+h)) \cos(\mu(x-x_p))\,\mathrm{d}\mu, \quad n \geq 1,\\ &= \frac{\cos(2n\theta_p)}{r_p^{2n}} + \sum_{m=0}^{\infty}A^{+}_{pp,mn}r_p^{2m}\ \cos(2m\theta_p),\end{aligned} \tag{38}$$

$$\begin{aligned}\varphi^{-}_{p,n} &= \frac{\sin((2n-1)\theta_p)}{r_p^{2n-1}} + \frac{1}{(2n-2)!}\int_0^{\infty}\hbar(\mu)\mu^{2n-2} \cosh(\mu(z+h))\ \sin(\mu(x-x_p))\,\mathrm{d}\mu, \quad n \geq 1,\\ &= \frac{\sin((2n-1)\theta_p)}{r_p^{2n-1}} + \sum_{m=1}^{\infty}B^{-}_{pp,mn}r_p^{2m-1}\ \sin((2m-1)\theta_p),\end{aligned} \tag{39}$$

with

$$A^{+}_{pp,mn} = \frac{1}{(2m)!\,(2n-1)!}\int_0^{\infty}\hbar(\mu)\mu^{2m+2n-1}\ \mathrm{d}\mu, \tag{40}$$

$$B^{-}_{pp,mn} = \frac{1}{(2m-1)!(2n-2)!}\int_0^{\infty}\hbar(\mu)\mu^{2m+2n-3}\ \mathrm{d}\mu, \tag{41}$$

where the path of each integration passes beneath the pole at $\mu = k$ for satisfying the far field radiation conditions.

Using the method given in O'Leary [41, Appendix] and Linton and McIver [34, Chapter 3.2.1], the multipoles singular at $(x, z) = (x_p, -h)$ can be expanded in terms of polar coordinate (r_q, θ_q):

$$\varphi^{+}_{p,n} = \sum_{m=0}^{\infty}A^{+}_{pq,mn}r_q^{2m}\ \cos(2m\theta_q) + \sum_{m=1}^{\infty}B^{+}_{pq,mn}r_q^{(2m-1)}\sin((2m-1)\theta_q), \quad p \neq q, \tag{42}$$

$$\varphi^{-}_{p,n} = \sum_{m=0}^{\infty}A^{-}_{pq,mn}r_q^{2m}\ \cos(2m\theta_q) + \sum_{m=1}^{\infty}B^{-}_{pq,mn}r_q^{(2m-1)}\ \sin((2m-1)\theta_q), \quad p \neq q, \tag{43}$$

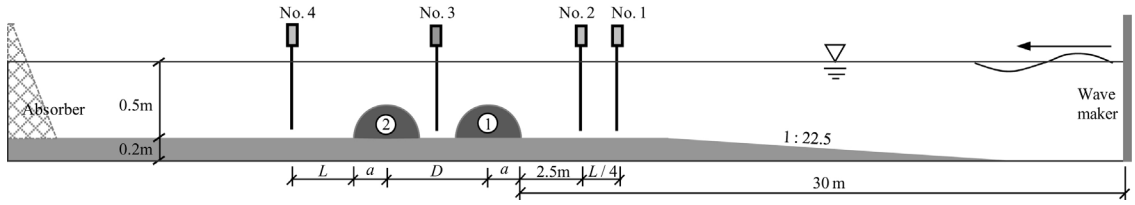

Fig. 2. Sketch of experimental set-up.

where the definitions of $A^{\pm}_{pq,mn}$ and $B^{\pm}_{pq,mn}$ are the same as that in Eqs. (19) and (20), but we have

$$P^{+}_{pq,mn} = \frac{(-1)^{n+m}(2n+2m-1)!}{(2m)!(2n-1)!(x_q-x_p)^{2n+2m}}, \tag{44}$$

$$P^{-}_{pq,mn} = \frac{(-1)^{n+m-1}(2n+2m-2)!}{(2m)!(2n-2)!(x_q-x_p)^{2n+2m-1}}, \tag{45}$$

$$Q^{+}_{pq,mn} = -\frac{2m}{2n-1}P^{-}_{pq,mn}, \tag{46}$$

$$Q^{-}_{pq,mn} = \frac{(-1)^{n+m-1}(2n+2m-3)!}{(2m-1)!(2n-2)!(x_q-x_p)^{2n+2m-2}}, \tag{47}$$

$$R^{+}_{pq,mn} = \frac{1}{(2m)!(2n-1)!}\int_0^{\infty}\hbar(\mu)\mu^{2m+2n-1}\cos(\mu(x_q-x_p))\,\mathrm{d}\mu, \tag{48}$$

$$R^{-}_{pq,mn} = \frac{1}{(2m)!(2n-2)!}\int_0^{\infty}\hbar(\mu)\mu^{2m+2n-2}\sin(\mu(x_q-x_p))\,\mathrm{d}\mu, \tag{49}$$

$$S^{+}_{pq,mn} = \frac{2m}{2n-1}R^{-}_{pq,mn}, \tag{50}$$

$$S^{-}_{pq,mn} = \frac{1}{(2m-1)!(2n-2)!}\int_0^{\infty}\hbar(\mu)\mu^{2m+2n-3}\cos(\mu(x_q-x_p))\,\mathrm{d}\mu. \tag{51}$$

In addition, we still define $A^{-}_{pp,mn} = B^{+}_{pp,mn} = 0$ as that in Eq. (29).

The velocity potential of normally incident waves is expanded using the Taylor expansion of exponential function:

$$\phi_{\mathrm{I}} = \mathrm{e}^{\mathrm{i}kx_q}\left[\sum_{n=0}^{\infty}\frac{(kr_q)^{2n}}{(2n)!}\cos(2n\theta_q) + \mathrm{i}\sum_{n=1}^{\infty}\frac{(kr_q)^{2n-1}}{(2n-1)!}\sin((2n-1)\theta_q)\right].$$

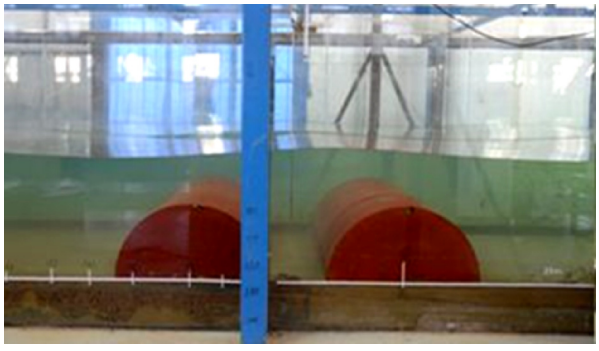

Fig. 3. A picture for two semi-circular bars in the wave flume at: $D = 0.83$ m (waves incident from right).

Inserting the velocity potential into Eq. (7), and using the same procedure as that of oblique waves, we have for $q = 1, 2, \ldots, N$:

$$\xi^{+}_{q,m}a_q^{-4m} - \sum_{p=1}^{N}\left(\sum_{n=1}^{\infty}\xi^{+}_{p,n}A^{+}_{pq,mn} + \sum_{n=1}^{\infty}\xi^{-}_{p,n}A^{-}_{pq,mn}\right) = \frac{k^{2m}}{(2m)!}\mathrm{e}^{\mathrm{i}k_x x_q}, \quad m \geq 1, \tag{53}$$

$$\xi^{-}_{q,m}a_q^{-4m+2} - \sum_{p=1}^{N}\left(\sum_{n=1}^{\infty}\xi^{+}_{p,n}B^{+}_{pq,mn} + \sum_{n=1}^{\infty}\xi^{-}_{p,n}B^{-}_{pq,mn}\right) = \frac{\mathrm{i}k^{2m-1}}{(2m-1)!}\mathrm{e}^{\mathrm{i}k_x x_q}, \quad m \geq 1. \tag{54}$$

Again, the above equations are solved by truncating m and n to M. The size of the linear system for normally incident waves is $2MN \times 2MN$.

As $x \to \pm\infty$, the multipoles for normally incident waves become [29, Eqs. (A.10) and (A.12)]:

$$\varphi^{+}_{p,n} \sim \frac{\mathrm{i}\pi k^{2n-1}}{2(2n-1)!N_0 h}\mathrm{e}^{\mp\mathrm{i}kx_p}\cosh(k(z+h))\mathrm{e}^{\pm\mathrm{i}kx}, \tag{55}$$

$$\varphi^{-}_{p,n} \sim \pm\frac{\pi k^{2n-2}}{2(2n-2)!N_0 h}\mathrm{e}^{\mp\mathrm{i}kx_p}\cosh(k(z+h))\mathrm{e}^{\pm\mathrm{i}kx}. \tag{56}$$

Then, the magnitudes of complex reflection and transmission coefficients are calculated by

$$C_R = |\tilde{R}| = \left|\sum_{p=1}^{N}\mathrm{e}^{\mathrm{i}kx_p}\left[\sum_{n=1}^{\infty}\xi^{+}_{p,n}\frac{\mathrm{i}\pi k^{2n-1}}{2(2n-1)!N_0 h} - \sum_{n=1}^{\infty}\xi^{-}_{p,n}\frac{\pi k^{2n-2}}{2(2n-2)!N_0 h}\right]\right|, \tag{57}$$

$$C_T = |\tilde{T}| = \left|1 + \sum_{p=1}^{N}\mathrm{e}^{-\mathrm{i}kx_p}\left[\sum_{n=1}^{\infty}\xi^{+}_{p,n}\frac{\mathrm{i}\pi k^{2n-1}}{2(2n-1)!N_0 h} + \sum_{n=1}^{\infty}\xi^{-}_{p,n}\frac{\pi k^{2n-2}}{2(2n-2)!N_0 h}\right]\right|. \tag{58}$$

The energy conversation relation in Eq. (37) still works for normally incident waves.

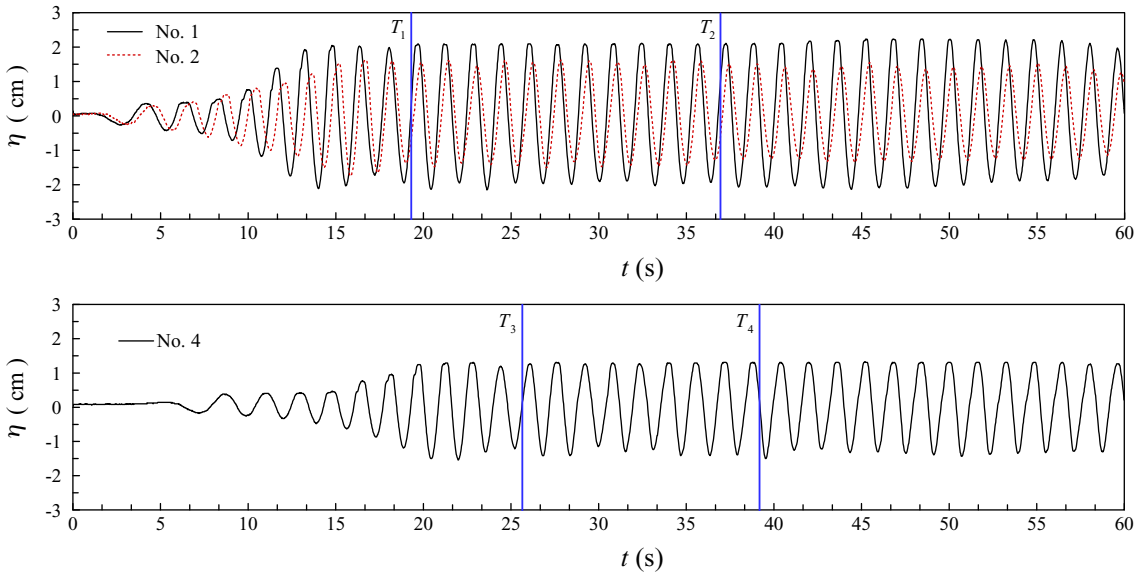

Fig. 4. Time histories of free surface elevations η measured by wave probes of Nos. 1, 2 and 4 for Case 2 at: $T = 1.6$ s and $D = 1.37$ m.

Table 1
Experimental cases and conditions.

Cases	Bar numbers	h (m)	a (m)	H/L	T (s)	D (m)
1	Single	0.5	0.3	0.01	1.0–2.2	–
2	Two	0.5	0.3	0.01	1.0–2.2	0.83, 1.37, 1.75
3	Two	0.5	0.3	0.01	1.2, 1.6, 2.0	0.7–3.2

4. Experimental tests

The reflection and transmission coefficients of single and two submerged semi-circular bars were measured in a wave-current flume (60 m long, 3 m wide and 1.5 m deep) in Shandong Provincial Key Laboratory of Ocean Engineering. A piston-type wave maker was equipped in the flume to generate required waves, and a sloping porous wave absorber was installed at the end of the flume to dissipate incident wave energy. The second half part of the flume was separated into two channels with 1.2 m wide and 1.8 m wide, respectively. The semi-circular bars made of steel plates were fixed in the 1.2 m wide channel. The water surface elevations around the bars were measured by four capacitive type wave probes named as Nos. 1–4. These wave probes were all calibrated in a small water tank before the tests, and had the accuracy of ±1 mm. The experimental set-up is shown in Fig. 2, and a picture for semi-circular bars in the flume is given in Fig. 3.

In our tests, the water depth h was 0.5 m, the wave steepness H/L (L is the wavelength) was fixed at 0.01, and the radius of each semi-circular bar was $a = 0.3$ m. All the experimental cases and conditions are listed in Table 1. The cases of $a = 0.4$ m and $H/L = 0.02$ were also examined in the tests. But for such cases, the wave nonlinear shoaling and breaking over bars had notable effects on the transmitted waves, and thus were not examined in the present linear analysis. For Case 1, the reflection and transmission coefficients of a single bar (only using Bar 1 in Fig. 2) were measured. But, two bars were examined in Cases 2 and 3. For Case 2, the spacing D between the centres of two bars was fixed at 0.83 m, 1.37 m and 1.75 m, respectively, and the incident wave period T were increased from 1.0 s to 2.2 s with an increasing step of 0.2 s. For Case 3, the wave period was fixed at 1.2 s, 1.6 s and 2.0 s, respectively, and the spacing D between two bars was varied from 0.7 m to 3.2 m (including 10–12 different values). In the tests, the positions of Bar 1 and No. 2 probe were fixed, and the spacing between them (from the bar front foot to probe) was 2.5 m. The position of No. 1 probe was changed to make the spacing between Nos. 1 and 2 probes always equal to $L/4$ for different incident waves. The position of Bar 2 was also changed according to desired values of D. No. 3 probe was placed at the

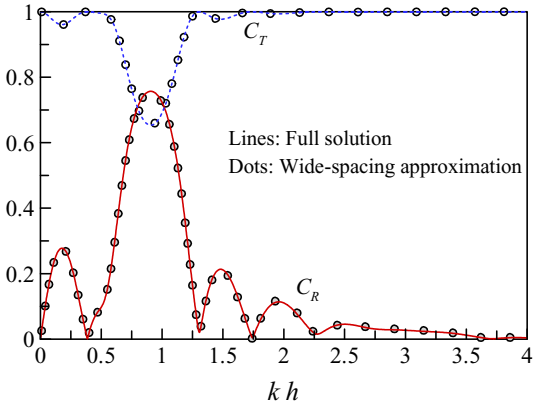

Fig. 5. Comparison between the full analytical solutions and the wide-spacing approximations for three bars at: $\beta = 0^\circ$, $a_1 = 0.5h$, $a_2 = 0.7h$, $a_3 = 0.6h$, $D_1 = 2.7h$ and $D_2 = 2.8h$.

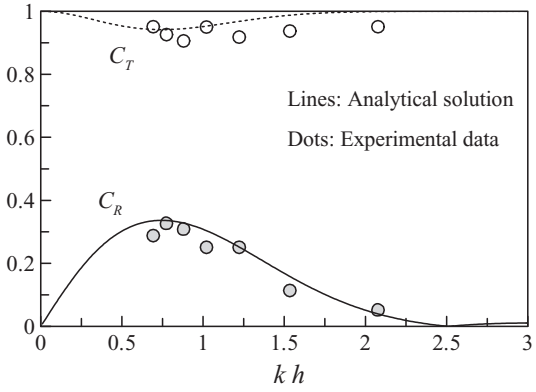

Fig. 6. Analytical and experiment results for a single semi-circular bar (Case 1).

middle position of two bars, and No. 4 probe was placed leaving about one wavelength from the back foot of Bar 2.

The free surface elevations measured by all wave probes were simultaneously recorded by a computer with a sampling frequency of 50 Hz. Typical time histories of free surface elevations are shown in Fig. 4. As shown in this figure, the stable surface elevations between T_1 and T_2 (measured by Nos. 1 and 2 probes) were selected to obtain the incident and reflected wave heights using Goda's method [42]. The stable surface elevation between T_3 and T_4 (measured by No. 4 probe) was selected to obtain the transmitted wave heights using the zero-up-cross analysis method. Then, the reflection and transmission coefficients were determined. In our tests, each case was repeated three times, and the averaged values were used.

5. Results

For the full solutions of obliquely and normally incident waves, a truncated number of $M=7$ has been adopted in all the calculations below. This can guarantee convergent results of reflection and transmission coefficients with four-figure accuracy. For all the results calculated by the full solutions, the energy conservation relation in Eq. (37) was accurately satisfied. The reflection and transmission coefficients calculated by the oblique wave solution in Section 3.1 at a very small wave incident angle were the same as that calculated by the normally incident wave solution in Section 3.2. In addition, we numerically solved the present boundary-value problem using the boundary element method (BEM) [43], and the agreement between the analytical solution and the BEM solution is rather good. All of these ensure that the solving procedure of the present solutions should be correct.

5.1. Comparisons between full solutions and wide-spacing approximations

When the semi-circular bars are widely spaced, approximated solutions can be obtained using the wide-spacing approximation [e.g., 34,39,44–47]. In such approximated method, only the full solution of a single bar is needed. Thus, the solving procedure is significantly simplified. Details on the wide-spacing approximations can be found in Linton and McIver [34, Chapter 6.3] and Linton [39, Section 2]. Linton [39] indicated that the resonant reflections for equally spaced identical bodies were most likely to occur when

$$\left|\cos(k_x D+\theta_T)\right|=1 \quad \text{or} \quad k_x D+\theta_T=n\pi, \quad n\geq 1, \tag{59}$$

where D is the spacing between adjacent bodies, and θ_T is the phase of the complex transmission coefficient of the single body with centre located at $(0, -h)$. Eq. (59) may be used to find the optimal spacing for maximum reflection when building equally spaced

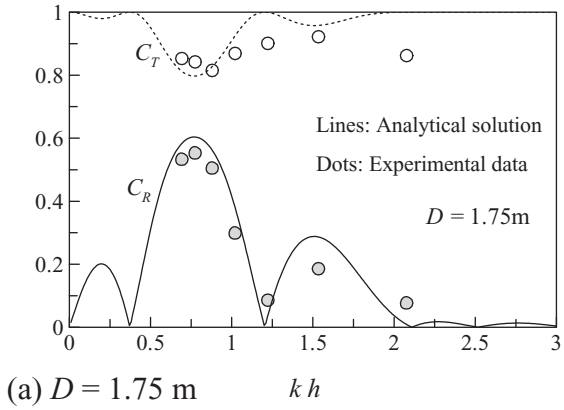

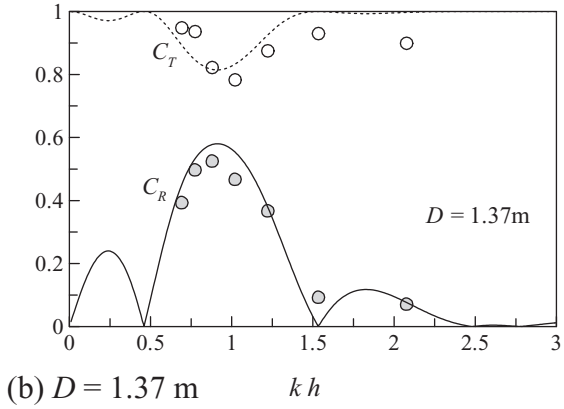

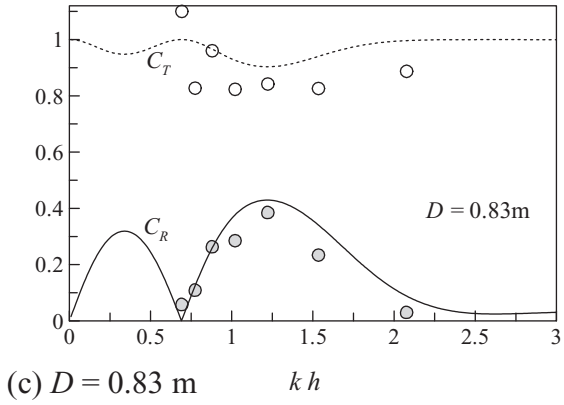

Fig. 7. Analytical and experimental results for two semi-circular bars (Case 2).

identical semi-circular bars. If the phase of complex transmission coefficient for a single bar is zero, Eq. (59) will be the Bragg's law of $k_x D=n\pi$.

The reflection and transmission coefficients, C_R and C_T, calculated by the full analytical solutions and the wide-spacing approximations are compared, and the typical results are given in Fig. 5. In this figure, we consider three bars with different radii: $a_1=0.5h$, $a_2=0.7h$ and $a_3=0.6h$. The waves are normally incident, and the spacings between adjacent bar centres are $D_1=2.7h$ and $D_2=2.8h$ (the spacing between adjacent bar foot edges is $1.5h$). We note from Fig. 5 that the agreement between the wide-spacing approximation and the full solution is excellent. If the bar

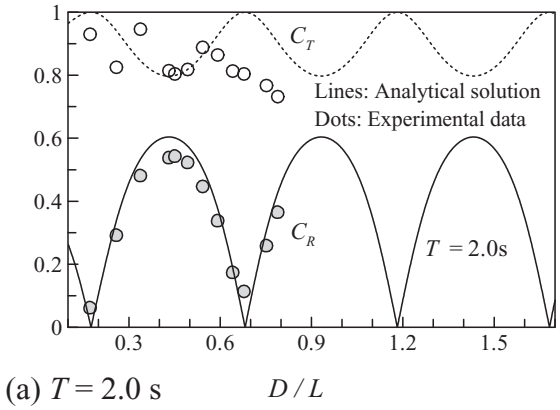

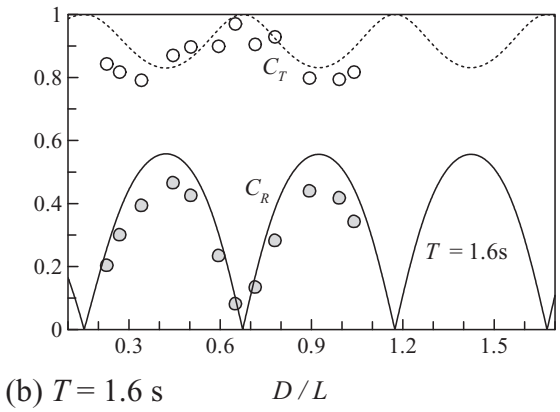

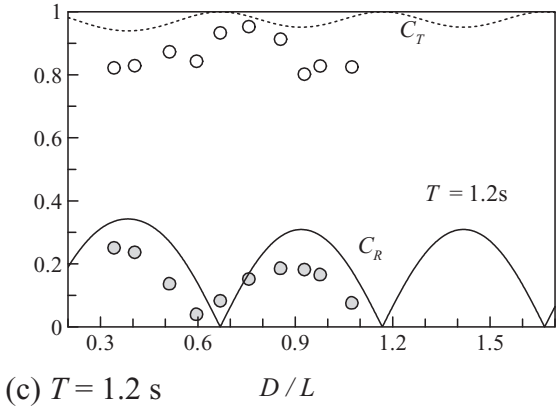

Fig. 8. Analytical and experimental results for two semi-circular bars (Case 3).

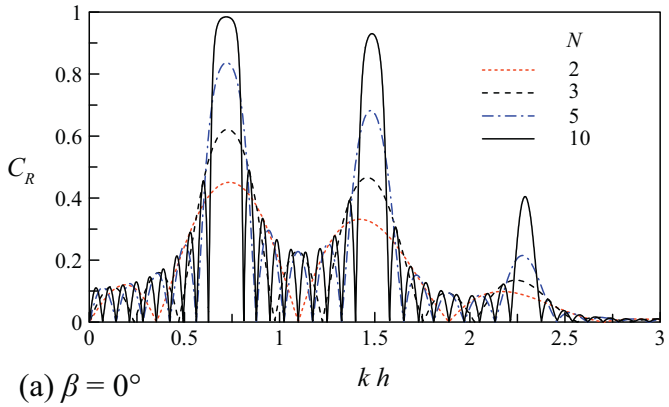

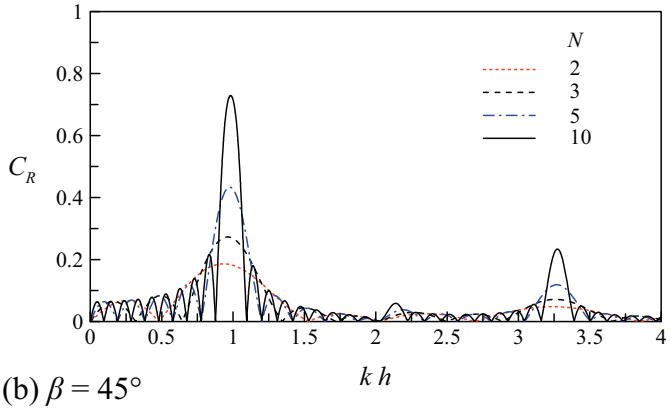

Fig. 9. Effect of the bar number N on C_R at: $a/h = 0.5$ and $D/h = 4.0$.

spacings further increase, the wide-spacing approximation will work better. For a Bragg reflection breakwater, the practical spacings between adjacent bodies should be relatively large. Then, the wide-spacing approximation can give good estimations of hydrodynamic quantities with significant saving of computing efforts.

5.2. Comparisons between analytical and experimental results

The reflection and transmission coefficients calculated by the full analytical solution are compared with that measured in the experimental tests. The compared results for three different cases are shown in Figs. 6–8. We note from these figures that the overall agreement between the analytical results and the experimental data is reasonable. Generally, the analytical results are slightly larger than the experimental data, as the energy dissipation in the tests cannot be modelled by the potential solution. For high frequency waves in Fig. 8c ($T = 1.2$ s), which may give rise to more pronounced damping effect in the tests, we can observe a shift towards the lower values of D/L for the experimental data in comparison with the analytical results. A somewhat similar phenomenon can also be found in Rey et al. [7] for wave motion over a single submerged bar with sharp corners. Further experimental study may be needed to understand the shift for the present smooth bars.

The resonant reflection by two semi-circular bars can be clearly observed in Figs. 7 and 8. Especially, when the wave period is fixed in Fig. 8, the reflection coefficient attains its local peaks periodically with the increasing relative bar spacing D/L. In comparison with the single semi-circular bar in Fig. 6, the two semi-circular bars in Figs. 7 and 8 can reflect more wave energies by wave interferences near two bars, and then bring better sheltering for leeside regions (lower transmission coefficient).

In Figs. 7 and 8, the resonant wave frequencies predicted by the analytical solution and measured by the model tests are in good agreement. In fact, these resonant frequencies also agree well with that predicted by the simple relation in Eq. (59), when the spacings between bars are relatively large. For example, the maximum reflection coefficient occurs at about $kh = 0.769$ in Fig. 7a. At this time, the phase of the complex transmission coefficient calculated by the full analytical solution of a single bar with centre located at $(0, -h)$ is about $\theta_T = 0.427$. Then, the value of $kD + \theta_T$ is about 0.993π, which is almost equal to π.

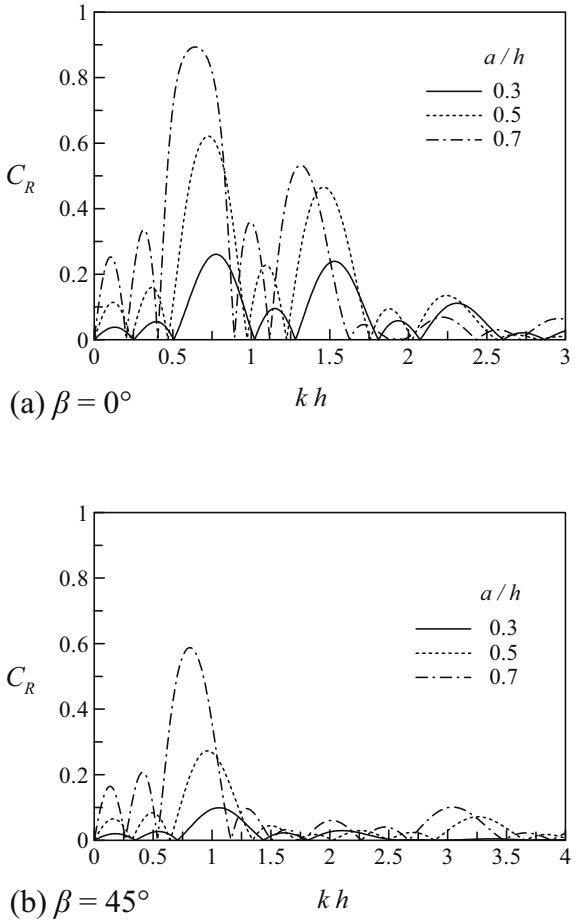

Fig. 10. Effect of the relative bar radius a/h on C_R at: $N = 3$ and $D/h = 4.0$.

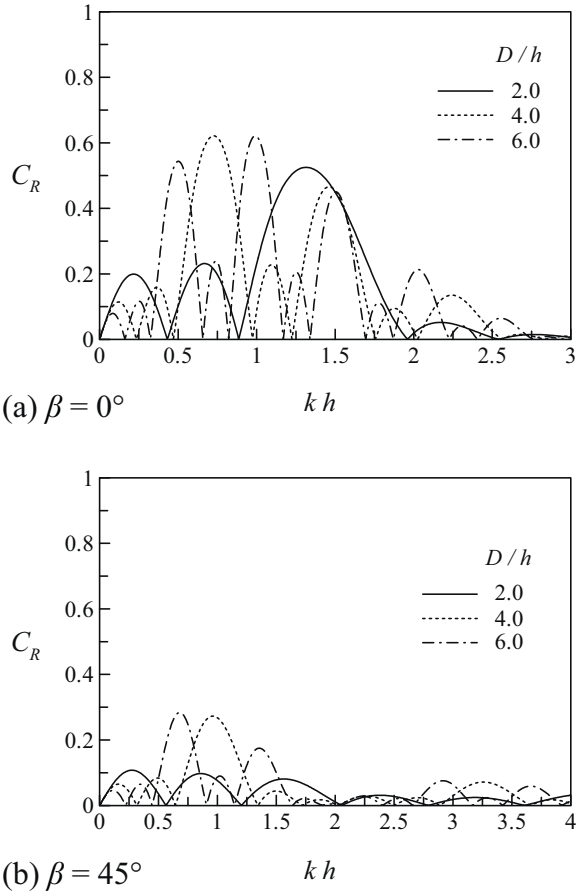

Fig. 11. Effect of the relative bar spacing D/h on C_R at: $N = 3$ and $a/h = 0.5$.

5.3. Discussions

A well-designed Bragg reflection breakwater is expected to effectively reflect wave energy in a wide range of wave frequencies. Thus, the maximum reflection coefficient and the corresponding bandwidth are of considerable interest for engineering designs. The effective bandwidth of Bragg reflection was defined by Bailard et al. [14] as the width of the principal wave reflection peak at the half value of the peak reflection coefficient. In this section, we will mainly examine the effects of various parameters on the reflection coefficient of multiple semi-circular breakwaters, especially the peak reflection coefficient and the bandwidth. The radii of semi-circular bars in all the following numerical examples are identical, and denoted by $a = a_p$ ($p = 1, 2, \ldots, N$). Except for Fig. 12, the spacings between adjacent semi-circular bars are also identical, and denoted by $D = D_p$ ($p = 1, 2, \ldots, N-1$).

We first examine the reflection coefficients of 2, 3, 5 and 10 identical semi-circular bars at $a/h = 0.5$ and $D/h = 4.0$. The results are plotted in Fig. 9. From Fig. 9a for normally incident waves, we note that when the bar number N increases, the peak reflection coefficient increases significantly and the bandwidth decreases. But, the effect of bar number N on the resonant frequency corresponding to the principle wave reflection peak is negligible. In addition, with the increasing bar number, the curves of reflection coefficients attain more zeros. Mei [2] has shown in theory that when the detuning frequency is less than the cut-off frequency, the reflection coefficients of periodic sandbars increase monotonically with the increasing bar number. Using the numerical results of integral matching methods, Belzons et al. [6] have also demonstrated that the peak reflection coefficient of periodic beds increases to unity with the increasing bed length. In Fig. 9a, the maximum reflection coefficient of 10 bars can attain 0.984 at about $kh = 0.720$. Such a large reflection coefficient is very favourable for submerged breakwaters. However, the corresponding bandwidth is not large. Also, the engineering costs become higher for more bars. Besides engineering costs, the bar number in practical design should be determined by the required both peak reflection coefficient and bandwidth. Similar phenomena as normally incident waves can also be observed in Fig. 9b for obliquely incident waves. The resonant reflection coefficient of multiple bars at $\beta = 45°$ is smaller than that at $\beta = 0°$.

The effects of the relative bar radius a/h and the relative bar spacing D/h on the reflection coefficient C_R are shown in Figs. 10 and 11, respectively. In these figures, three identical semi-circular bars are examined. We note from Fig. 10 that with the increasing bar radius, the peak reflection coefficient increases significantly and the corresponding resonant frequency decreases. So, larger semi-circular bars are more efficient for reflecting longer waves, which should be natural in physics. We note from Fig. 11 that when the relative bar spacing D/h increases from 2.0 to 6.0, the resonant frequency decreases a lot, but the change of the peak reflection coefficient is small. From Fig. 11a, it is interesting to find that for the case of $D/h = 6.0$, the second resonant reflection coefficient at $kh = 0.991$ ($kD + \theta_T = 1.992\pi$) becomes larger than the first resonant reflection coefficient at $kh = 0.502$ ($kD + \theta_T = 1.027\pi$). But, both bandwidths are small. It seems from Fig. 11a that the cases of $D/h = 2.0$ and 4.0 are better than the case of $D/h = 6.0$ as they can reflect more wave

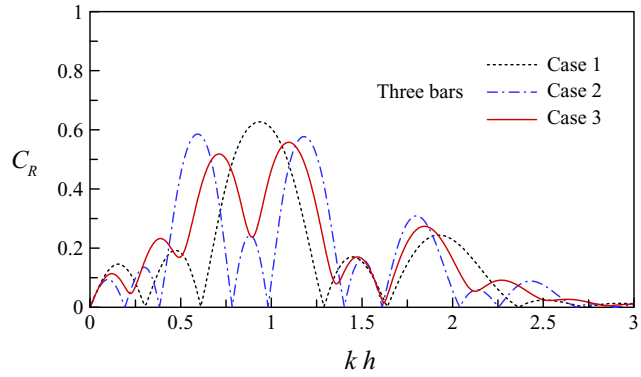

(a) Case 1, $D_1 = D_2 = 3h$; Case 2, $D_1 = D_2 = 5h$; Case 3, $D_1 = 5h$ and $D_2 = 3h$

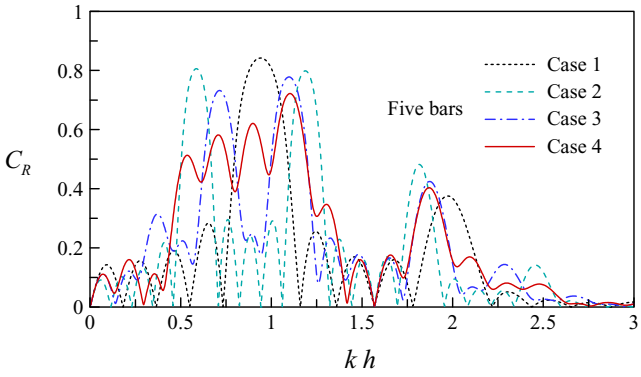

(b) Case 1, $D_1 = D_2 = D_3 = D_4 = 3h$; Case 2, $D_1 = D_2 = D_3 = D_4 = 5h$; Case 3, $D_1 = D_3 = 5h$ and $D_2 = D_4 = 3h$; Case 4, $D_1 = D_2 = 5h$ and $D_3 = D_4 = 3h$

Fig. 12. Effect of the bar spacing arrangement on C_R at: $\beta = 0^\circ$ and $a/h = 0.5$.

energies in a wider range of wave frequencies. In practice, one may adjust the bar spacings according to different design wave periods.

In Fig. 11, the spacings between adjacent bars are identical. Bailard et al. [14] and Hsu et al. [16] have shown that the bandwidth of Bragg reflection could be increased by setting non-identical bar spacings. So, we use Fig. 12 to further examine the effect of bar spacing arrangement on the Bragg reflection. In Fig. 12a, the reflection coefficients of three semi-circular bars with different spacing arrangements are presented. The Cases 1 and 2 in Fig. 12a have identical spacings of $3h$ and $5h$, respectively. However, the bar spacings of Case 3 are $D_1 = 5h$ and $D_2 = 3h$. The case of $D_1 = 3h$ and $D_2 = 5h$ is not considered, as its reflection coefficient magnitude is the same as that of Case 3 according to reciprocity relations [34, Eq. (1.63)]. We note from Fig. 12a that the resonant reflection frequency of Case 3 occurs between that of Cases 1 and 2. In addition, the peak reflection coefficient of Case 3 is slightly smaller than that of Cases 1 and 2. The benefit of using bars with non-identical spacings cannot be clearly observed in Fig. 12a. Now we observe Fig. 12b for five semi-circular bars with different spacing arrangements. The Cases 1 and 2 in Fig. 12b still have identical spacings of $3h$ and $5h$, respectively. For the Case 3, the bar spacings are periodically changed, i.e., $D_1 = 5h$, $D_2 = 3h$, $D_3 = 5h$ and $D_4 = 3h$. For the Case 4, the bar spacings are divided into two groups, i.e., $D_1 = D_2 = 5h$ and $D_3 = D_4 = 3h$. We note from Fig. 12b that the Case 3 with periodically changed bar spacings may not be a better wave reflector compared to Cases 1 and 2 with identical bar spacings. But, the reflection coefficient of Case 4 is not less than about 0.4 in a very wide range of $kh = 0.5$–1.2. This should be very useful for Bragg reflection breakwaters. When a large bandwidth of Bragg reflection is required, the bar spacings may be arranged by referring Case 4 in Fig. 12b.

In preceding Figs. 9–11, the reflection coefficients of oblique waves are examined at a fixed angle of $\beta = 45^\circ$. In such a wave incident angle, the reflection coefficients of oblique waves are generally smaller than that of normally incident waves. Now, we use Fig. 13 to directly show the variation of the reflection coefficient versus the wave incident angle. We note from Fig. 13a that when the wave incident angle increases, the reflection coefficient of a single semi-circular bar first decreases, attains its zero and then approaches unity. This is in fact the common feature of oblique wave reflection by a single submerged bottom-standing structure. But for multiple semi-circular bars in Fig. 13b, the variation of the reflection coefficient versus wave incident angle becomes rather complicated due to wave interferences among bars. When the wave incident angle increases from 0° to 90°, the reflection coefficient of three bars first decreases, attains its first zero, then oscillates between its local peaks and zeros, and finally rapidly approaches unity.

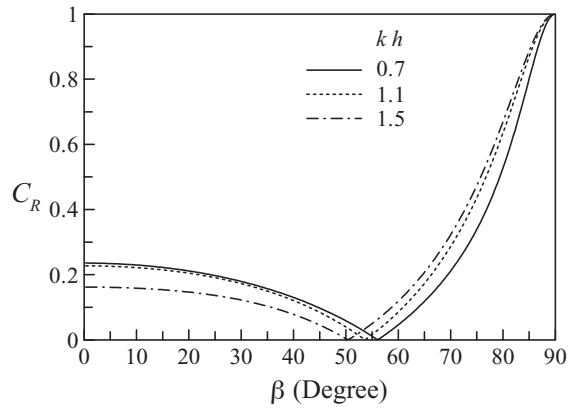

(a) A single bar ($N = 1$)

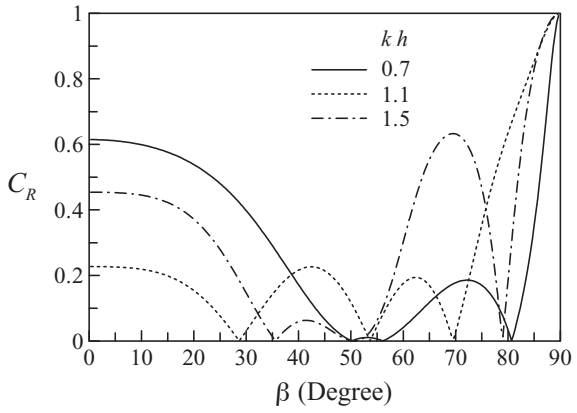

(b) Three bars ($N = 3$)

Fig. 13. Effect of the wave incident angle β on C_R: $a/h = 0.5$ and $D/h = 4.0$.

6. Conclusions

We have developed full linear potential solutions for Bragg reflection of water waves by a series of submerged semi-circular bars using multipole expansions and the shift of polar coordinates. The obliquely and normally incident waves have been independently considered. We have compared the full solutions of multiple bars with the wide-spacing approximations, which only need the full solution of a single bar. The agreement between the full solutions and the wide-spacing approximations is excellent when the spacing between adjacent bar foot edges is not less than 1.5 times water depth. Also, we have measured the reflection and transmission coefficients of submerged semi-circular bars at different wave periods and bar spacings in a laboratory wave flume. The calculated reflection and transmission coefficients agree reasonably well with the experimental data.

The effects of the bar number and radius, the arrangement of bar spacing and the wave incident angle on the Bragg reflection have been examined. The peak reflection coefficient significantly increases with the increasing bar number, while the corresponding bandwidth decreases. When the bar radius increases, the peak reflection coefficient increases and the resonant frequency decreases. The resonant frequency decreases with the increasing bar spacing. Five identical bars ($a = 0.5h$) with suitably designed spacings ($D_1 = D_2 = 5h$ and $D_3 = D_4 = 3h$) can guarantee the reflection coefficient no less than about 0.4 in a wide range of $kh = 0.5$–1.2. This is very favourable for practical coastal protections. The effect of the wave incident angle on the reflection coefficient is rather complicated, and should be analysed according to different design conditions.

Acknowledgment

This work was supported by the National Natural Science Foundation of China (Grant Nos. 51490675, 51322903 and 51279224).

References

[1] Davies AG, Heathershaw AD. Surface-wave propagation over sinusoidally varying topography. J Fluid Mech 1984;144:419–43.
[2] Mei CC. Resonant reflection of surface water waves by periodic sandbars. J Fluid Mech 1985;152:315–35.
[3] Kirby JT. A general wave equation for waves over rippled beds. J Fluid Mech 1986;162:171–86.
[4] Mei CC, Hara T, Naciri M. Note on Bragg scattering of water waves by parallel bars on the seabed. J Fluid Mech 1988;186:147–62.
[5] Guazzelli E, Rey V, Belzons M. Higher-order Bragg reflection of gravity surface waves by periodic beds. J Fluid Mech 1992;245:301–17.
[6] Belzons M, Rey V, Guazzelli E. Subharmonic Bragg resonance for surface water waves. Europhys Lett 1991;16(2):189–94.
[7] Rey V, Belzons M, Guazzelli E. Propagation of surface gravity waves over a rectangular submerged bar. J Fluid Mech 1992;235:453–79.
[8] Rey V. A note on the scattering of obliquely incident surface gravity waves by cylindrical obstacles in waters of finite depth. Eur J Mech B/Fluids 1995;14(2):207–16.
[9] Cho YS, Lee C. Resonant reflection of waves over sinusoidally varying topographies. J Coast Res 2000;16(3):870–6.
[10] Athanassoulis GA, Belibassakis KA. A consistent coupled-mode theory for the propagation of small-amplitude water waves over variable bathymetry regions. J Fluid Mech 1999;389:275–301.
[11] Porter R, Porter D. Scattered and free waves over periodic beds. J Fluid Mech 2003;483:129–63.
[12] Belzons M, Guazzelli E, Parodi O. Gravity waves on a rough bottom: experimental evidence of one-dimensional localization. J Fluid Mech 1988;186:539–58.
[13] Mattioli F. Resonant reflection of a series of submerged breakwaters. Il Nuovo Cimento C 1990;13(5):823–33.
[14] Bailard JA, DeVries JW, Kirby JT. Considerations in using Bragg reflection for storm erosion protection. J Waterw Port Coast Ocean Eng 1992;118(1):62–74.
[15] Mase H, Oki SI, Takeba K. Wave equation over permeable rippled bed and analysis of Bragg scattering of surface gravity waves. J Hydraul Res 1995;33(6):789–812.
[16] Hsu TW, Tsai LH, Huang YT. Bragg scattering of water waves by multiply composite artificial bars. Coast Eng J 2003;45(2):235–53.
[17] Cho YS, Lee JI, Kim YT. Experimental study of strong reflection of regular water waves over submerged breakwaters in tandem. Ocean Eng 2004;31(10):1325–35.
[18] Twu SW, Liu CC. Interaction of non-breaking regular waves with a periodic array of artificial porous bars. Coast Eng 2004;51(3):223–36.
[19] Lan YJ, Hsu TW, Lai JW, Chang CC, Ting CH. Bragg scattering of waves propagating over a series of poro-elastic submerged breakwaters. Wave Motion 2011;48(1):1–12.
[20] Zhang JS, Jeng DS, Liu PLF, Zhang C, Zhang Y. Response of a porous seabed to water waves over permeable submerged breakwaters with Bragg reflection. Ocean Eng 2012;43:1–12.
[21] Karmakar D, Guedes Soares C. Wave transformation due to multiple bottom-standing porous barriers. Ocean Eng 2014;80:50–63.
[22] Liu HW, Luo H, Zeng HD. Optimal collocation of three kinds of Bragg breakwaters for Bragg resonant reflection by long waves. J Waterw Port Coast Ocean Eng 2014;141(3):04014039.
[23] Aburatani S, Koizuka T, Sasayama H, Tanimoto K, Namerikawa N. Field test on a semi-circular caisson breakwater. Coast Eng J 1996;39(1):59–78.
[24] Xie SL. Waves forces on submerged semicircular breakwater and similar structures. China Ocean Eng 1999;13(1):63–72.
[25] Mallayachari V, Sundar V. Wave transformation over submerged obstacles in finite water depths. J Coast Res 1996;12(2):477–83.
[26] Yuan DK, Tao JH. Wave forces on submerged, alternately submerged, and emerged semicircular breakwaters. Coast Eng 2003;48(2):75–93.
[27] Zhang NC, Wang LQ, Yu YX. Oblique irregular waves load on semicircular breakwater. Coast Eng J 2005;47(4):183–204.
[28] Dhinakaran G, Sundar V, Sundaravadivelu R. Review of the research on emerged and submerged semicircular breakwaters. Proc Inst Mech Eng M: J Eng Marit Environ 2012;226:397–409.
[29] Liu Y, Li HJ. Analysis of wave interaction with submerged perforated semi-circular breakwaters through multipole method. Appl Ocean Res 2012;34:164–72.
[30] Liu Y, Li HJ. Analysis of oblique wave interaction with a submerged perforated semicircular breakwater. J Eng Math 2013;83(1):23–36.
[31] Ursell F. On the heaving motion of a circular cylinder on the surface of a fluid. Q J Mech Appl Math 1949;2(2):218–31.
[32] Thorne RC. Multipole expansions in the theory of surface waves. Proc Camb Philos Soc 1953;49(4):707–16.

[33] Wu GX, Eatock Taylor R. The second order diffraction force on a horizontal cylinder in finite water depth. Appl Ocean Res 1990;12(3):106–11.
[34] Linton CM, McIver P. Handbook of mathematical techniques for wave/structure interactions. Boca Raton: Chapman & Hall/CRC; 2001.
[35] Shen YM, Zheng YH, Ng CO. Interaction of oblique waves with an array of long horizontal circular cylinders. Sci China Ser E 2007;50(4):490–509.
[36] Chapman GJD [Ph.D. thesis] A weakly singular integral equation approach for water wave problems. United Kingdom: University of Bristol; 2005.
[37] Evans DV, Jeffrey DC, Salter SH, Taylor JRM. Submerged cylinder wave energy device: theory and experiment. Appl Ocean Res 1979;1(1):3–12.
[38] Wu GX, Eatock Taylor R. The hydrodynamic force on an oscillating ship with low forward speed. J Fluid Mech 1990;211:333–53.
[39] Linton CM. Water waves over arrays of horizontal cylinders: band gaps and Bragg resonance. J Fluid Mech 2011;670:504–26.
[40] Gradshteyn IS, Ryzhik IM. Table of integrals, series, and products. 7th ed. New York: Academic Press; 2007.
[41] O'Leary M. Radiation and scattering of surface waves by a group of submerged, horizontal, circular cylinders. Appl Ocean Res 1985;7(1):51–7.
[42] Goda Y, Suzuki Y. Estimation of incident and reflected waves in random wave experiments. In: Proceedings of the 15th coastal engineering conference. 1976. p. 828–45.
[43] Liu Y, Li HJ, Li YC. A new analytical solution for wave scattering by a submerged horizontal porous plate with finite thickness. Ocean Eng 2012;42:83–92.
[44] Newman JN. Propagation of water waves past a long two-dimensional obstacle. J Fluid Mech 1965;23:23–9.
[45] Evans DV. The wide spacing approximation applied to multiple scattering and sloshing problems. J Fluid Mech 1990;210:647–58.
[46] Porter R, Evans DV. Scattering of flexural waves by multiple narrow cracks in ice sheets floating on water. Wave Motion 2006;43(5):425–43.
[47] McIver P. An extended wide-spacing approximation for two-dimensional water-wave problems in infinite depth. Q J Mech Appl Math 2014;67(3):445–68.